Direct Use of the High Impedance Surface as an Antenna Without Dipole on Top

Caner Guclu, *Student Member, IEEE*, Jeff Sloan, *Student Member, IEEE*, Shiji Pan, *Student Member, IEEE*, and Filippo Capolino, *Senior Member, IEEE*

***Abstract*—High impedance surfaces (HISs) have been proposed and used as substrate for dipoles for realizing low-profile antennas. Here, we show that HISs can be used directly as low-profile antennas with a single feed point, without any dipole on top. The structure is made of only two metallic layers, the patterned surface and the ground plane below, at a subwavelength distance. We analyze two possible feeding mechanisms of an HIS made of dogbone-shaped conductors, though the ideas proposed here can be applied also to other HIS structures. We show that broadside gain of the order of 7–11 dBi can be obtained. We also explain that radiation of the HIS is in part related to a TM-like leaky wave with attenuation constant that is not as small in contrast to other standard high-gain leaky-wave antennas.**

***Index Terms*—Artificial magnetic conductor (AMC), dogbones, high impedance surface (HIS), leaky-wave antennas, low-profile antennas, planar antennas.**

I. Introduction

PLANAR antennas are desirable for their low profile and fabrication advantages. For this purpose, ground planes are used for confining the radiated power to a hemisphere and increasing the directivity, as well as a shielding mechanism. Conceptually, metamaterials and metalayers contributed to the planarization of antennas. Grounded substrates composed of artificial magnetic conductors (AMCs) or more generally high impedance surfaces (HISs) increase the forward (broadside) gain and the radiation efficiency of transverse dipole antennas. Placing a dipole on an HIS may be advantageous compared to directly locating a transverse dipole at a subwavelength distance over a ground plane since the tangential electrical field is not constrained to vanish on the plane, as shown in several studies (see [1]–[4] and references therein). For example, [1] reports an HIS made of the mushroom-like structure [5], used to enhance the efficiency of a proximity dipole. In [2], a dipole antenna over an HIS of square patches is used for miniaturization and bandwidth enhancement. Similarly a bow-tie antenna above a mushroom-like substrate was shown in [3]. More recently in [4], with a fully planar implementation, an HIS of planar dogbones was used to improve the performance of a folded dipole antenna. In [6], the radiating modes in a mushroom-type HIS are excited by a dipole on top. These and similar studies, like those in their references, made it possible to decrease the thickness of a grounded transverse dipolar antenna. However, even fully planar realizations of a dipole on top of an HIS as in [4] require three metallic layers. In this letter, it is shown that HISs can be used directly as a radiator, with single feed point, and without any dipole on top, thus eliminating one metal layer.

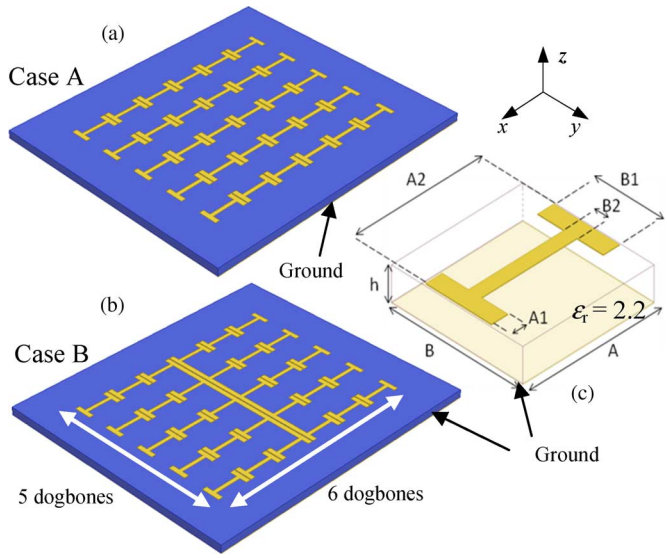

Fig. 1. Direct use of the HIS as a low-profile antenna, and two possible feeding mechanisms. The HIS is made by a patterned metallic surface on a grounded substrate. (a) The HIS antenna is fed at the gap between the dogbones at the center (Case A). (b) The HIS antenna is fed by a twin line (Case B). (c) Unit cell with quotes.

Similar ideas have been shown in conference proceedings as in [7] and [8]. In [7], the proposed HIS structure was made of square patches with vias (i.e., mushrooms as in [5]) and fed by one of the vias. In [8], a fully planar HIS (as in Case A, Fig. 1) was proposed made by dogbone-shaped conductors over a ground plane. The HIS resonance of dogbones over a ground plane is related to the antisymmetric current distribution in metalayers made of pairs of dogbones as shown in [9] and [10], which is associated to artificial magnetism. Therefore, the resonance frequency of the HIS is strictly related to the magnetic resonance studied in [9] and [10], as explained in [4].

Instead of using the HIS as a pure magnetic reflector, we use the HIS directly as a radiating low-profile antenna, utilizing only two metal layers. We also show the underlying physical radiation mechanism that is based on the ability of the HIS to support leaky waves (LWs), in the proximity of the magnetic resonance, as was shown in [11] for a metalayer made of pairs as in [9]

Manuscript received October 26, 2011; revised December 09, 2011; accepted December 14, 2011. Date of publication December 21, 2011; date of current version January 30, 2012. This work was supported in part by the Semiconductor Research Corporation (SRC)-GRC under Grant 2009-VJ-1962.

The authors are with the Department of Electrical Engineering and Computer Science, University of California, Irvine, Irvine, CA 92697 USA (e-mail: f.capolino@uci.edu).

Color versions of one or more of the figures in this letter are available online at http://ieeexplore.ieee.org.

Digital Object Identifier 10.1109/LAWP.2011.2181148

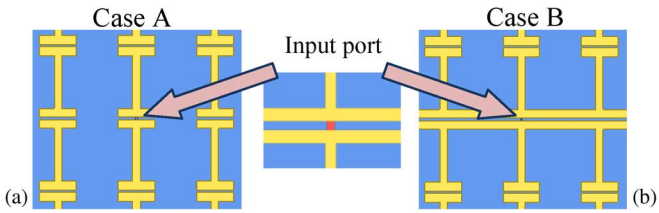

Fig. 2. Lumped port excitation in the gap between two dogbones at the center of the antennas for (a) Case A and (b) Case B.

and [10]. In fact, the authors observed that in the design of a dipole antenna over an HIS, as reported in [4], certain sidelobes appear in the E-plane, with beam pointing angle increasing with frequency, as is typical of forward LW radiation [12]. This was a hint that the real radiation mechanism of dipole over the HIS was not purely that of a magnetic mirror. One should note that the field produced by a dipole over a patterned surface consists of the so-called "spatial field" contribution, which is subject to reflection due to a magnetic mirror, and also by modal fields (bound and leaky waves). In this letter, we show that the term due to the modal field plays an important role. For comparison purposes, we choose the same HIS as in [4] where the HIS was used as a substrate for a folded dipole (exact dogbone dimensions and more or less the same overall HIS size). Therefore, here, as in [4], the dogbone-shaped conductors have dimensions (in millimeters) $A = B = 7$, $A1 = 0.875$, $A2 = 6.83$, $B1 = 3.5$, $B2 = 0.7$, over a Duroid substrate ($\varepsilon_r = 2.2$) with thickness $h = 1.6$ mm. The ground and dogbone conductors are made of 35-μm-thick copper with conductivity 5.8×10^7 S/m. The frequency at which the plane-wave reflection coefficient from the HIS has zero-phase is 6.75 GHz (also called magnetic resonance). It should be stressed that the proposed antenna is not a conventional leaky-wave antenna, based on having a very small LW attenuation constant a, as that studied in [13] for instance. Note also that in high-gain Fabry–Perot cavity LW antennas, as those in [13], the thickness is much larger than the one considered in this letter.

II. Design and Analysis

The HIS antennas in Fig. 1(a) and (b) are made of dogbones shown in Fig. 1(c). Two types of feeding configurations are investigated and shown in Fig. 2: Case A and Case B. In Case B, a twin line is used to connect the central row of dogbones. The metal strips of the twin line have width $A1$. In both HIS antenna designs, the feed is a lumped port placed in the gap between two contiguous dogbones (Fig. 2), at the center of the antenna that is simulated with Ansoft HFSS. The twin line is used to improve the broadside gain by improving the excitation of parallel linear arrays of dogbones (chains). This is compared to Case A and explained later on.

The broadside gains of Cases A and B are plotted versus frequency in Fig. 3. HFSS and Ansoft Designer provide an overall agreement, besides a frequency shift, cross-validating the simulated radiation performance of the HIS antenna (all other results in the letter are obtained with HFSS). Case A provides 7.5–10 dBi gain over a band from 5 to 6.7 GHz. Case B provides a wide gain band from 5.5 to 7.6 GHz with gain values between 7.5 and 12.6 dBi. The sharp decrease in the broadside gain

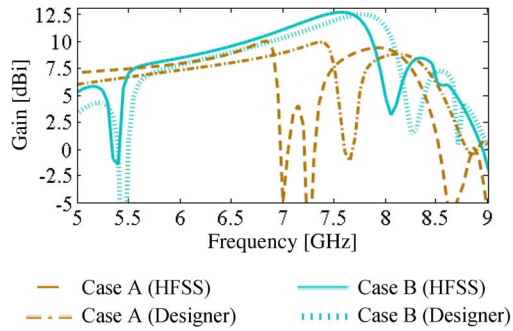

Fig. 3. Broadside gain with respect to frequency. HFSS results are compared to those from Ansoft Designer.

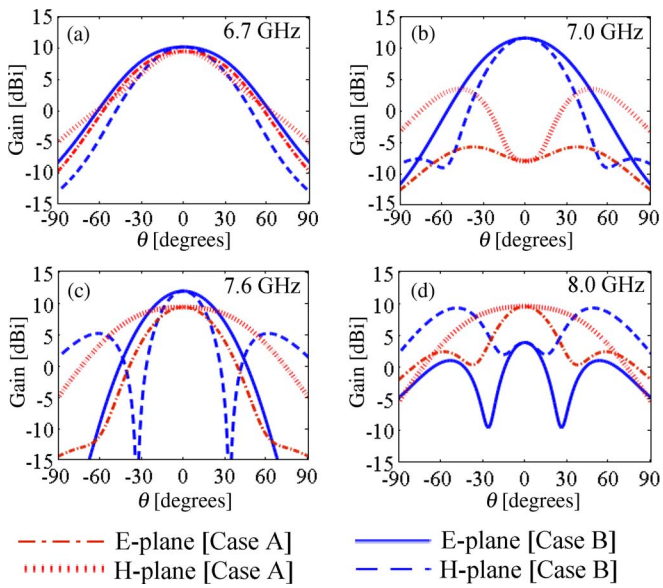

Fig. 4. E-plane and H-plane gain pattern at (a) 6.7, (b) 7.0, (c) 7.6, and (d) 8.0 GHz.

at 5.4 GHz for Case B is due to opposite-phase currents in the adjacent chains, whereas a similar phenomenon occurs around 7 GHz for Case A. The two antennas show similar gain trends from 5 to 6.9 GHz, where Case A reaches the maximum gain of 9.9 dBi. However, the gain of Case B continues to grow to the maximum of 12.6 dBi at 7.6 GHz. We conclude that from the point of view of maximizing gain, the twin line feeding apparently improves the HIS antenna performance. The comparison of gain patterns in both E- and H-planes of the two HIS antennas is provided in Fig. 4 at 6.7, 7, 7.6, and 8 GHz. At 6.7 GHz, both Case A and B exhibit similar radiation patterns with a maximum at broadside. At 7 GHz, the radiation pattern for Case A exhibits two maxima in the H-plane around 47° from broadside. Indeed, the sharp decrease in Fig. 3 of the broadside gain at 7 GHz (for Case A) is related to the appearance of lateral beams. Case B exhibits a radiation pattern with a maximum at broadside beyond 7 GHz. At 7.6 GHz, Case A exhibits a gain maximum at broadside, whereas Case B has sidelobes at 60° in the H-plane. At 8 GHz, even stronger sidelobes are present for Case B in both planes and especially in the H-plane. The difference of gain and radiation patterns in Cases A and B is associated with the different ways that the adjacent chains of dogbones are fed.

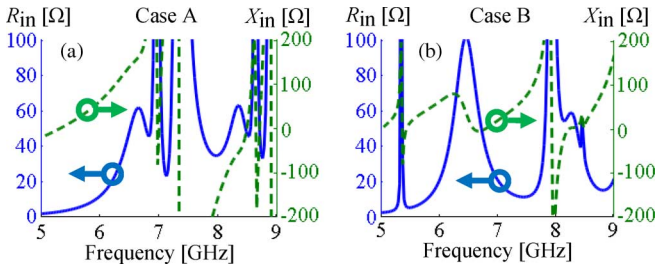

Fig. 5. Input impedance $R_{\rm in} + jX_{\rm in}$ for (a) Case A and (b) Case B.

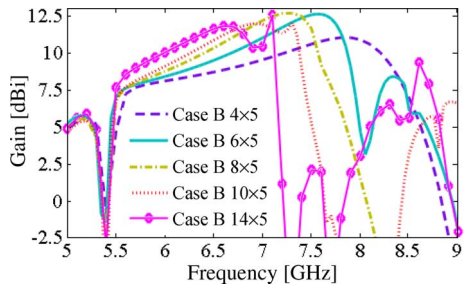

Fig. 6. Broadside gain versus frequency, by changing the number of HIS elements along the x-direction (for instance, 6 means three dogbones on each side of the feed, as in Fig. 1). Increasing the number of elements causes the sudden gain drop at lower frequencies.

In Case B, the phase of excitation of the lateral dogbone chains is still almost in phase at frequencies up to 7.6 GHz to cause the gain increase and the presence of the radiation maximum at broadside.

The lumped-port input impedance for Cases A and B is plotted in Fig. 5. Near 6.2 GHz, the input resistance and reactance of Case A changes slowly, showing that this is a promising band for matching and also has desirable gain levels. The elimination of the inductive input reactance requires further investigation for input matching. The input impedance of Case B has two frequency bands in which the real part has low variation with frequency: 1) around 5.5 GHz, Case B exhibits low reactance with gain of the order of 7.5 dBi; 2) around 6.8–7.6 GHz, Case B still exhibits slowly varying impedance with gain in the range of 10–12 dBi. Also, the input reactance is lower compared to Case A. To conclude, Case B seems more favorable to be matched, and it exhibits a wider band of broadband gain. A twin line may be exploited for feeding and matching Case B; a coaxial feed from the bottom can be used for feeding both Cases A and B.

A layer of dogbones in periodic arrangement can support TM-like leaky modes along the dogbone chains (i.e., in the x-direction, Fig. 1), as was also proved in [11]. Radiation from the HIS is surely affected by the number of HIS elements in the direction of LW propagation, especially when only a few elements are used. This is shown in Fig. 6 for the promising HIS antenna "Case B" by varying the number of dogbones in the chains and keeping the number of chains fixed at 5.

When the number of dogbones in the chains is increased, the dip after the gain peak moves to lower frequencies, as plotted in Fig. 6. Also, the maximum broadside gains of Case B 6×5 and 8×5 designs are pretty high: 12.6 dBi at 7.6 GHz and 12.7 dBi

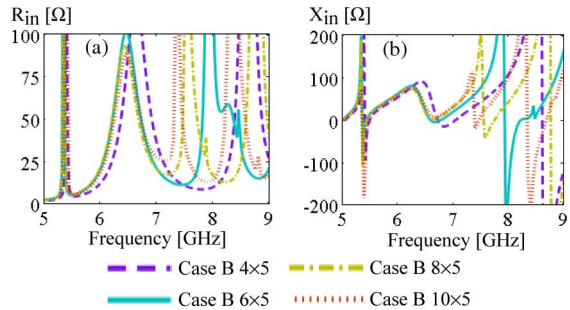

Fig. 7. (a) Real and (b) imaginary part of the input impedance $R_{\rm in} + jX_{\rm in}$ for Case B design, with 4×5, 6×5, 8×5, and 10×5 dogbones.

at 7.3 GHz, respectively. This result implies that it is better to have at least a few dogbones along x, though increasing the number of dogbones in a chain, to more than 6 for example, does not improve the broadside gain considerably. This means that most of the radiation is due to the currents flowing in the first three dogbones close to the excitation port.

The real and imaginary parts of the input impedance of Case B with 4×5, 6×5, 8×5, and 10×5 dogbones are plotted in Fig. 7. In all these cases, there are two regions that are important for stable input matching. The first one is around 6 GHz, where all the curves show more or less the same impedance and same gain values (Fig. 6). The second one is the frequency region where the real part of the input impedance for the aforementioned four designs exhibits flat regions. This happens between the two resonances: one at 6.5 GHz and the higher one in the range 7.4–8 GHz, depending on the number of dogbones along the x-direction. Note that this latter resonance corresponds to the sudden gain drop shown in Fig. 6. In this second frequency band, the bandwidth of the flat real part of the input impedance decreases with increasing number of dogbones. In this region, the imaginary part of the input impedances is not far from vanishing for all the cases. In conclusion, increasing the number of dogbones to more than six elements in the chains does not significantly improve the gain and causes degradation in the bandwidth of input matching in the second frequency region.

The radiation mechanism of the HIS antenna is now further analyzed by exploring the TM-like LW in the HIS, propagating along the x-direction (Fig. 1). We have already observed in Fig. 6 that the plot of gain versus frequency tends to stabilize when increasing the number of elements in the x-direction. This behavior is now clarified by plotting the x-component of the electric field in the gap between consecutive dogbones, versus dogbone number, as in Fig. 8. This HIS is made of 30 dogbone elements along the x-direction, and periodic boundary conditions are used along the y-direction in the HFSS simulations. The first dogbone in the row is excited by a lumped port. These curves show that the field decays with a clear exponential trend for the first dogbone elements, revealing the presence of an LW. At 5.5 GHz, after element 4, the LW field is already decayed 25 dB, and other modes or the spatial field generated by the excitation become dominant. Instead, at 6.5 GHz, the LW decays with a smaller attenuation constant α, and the exponential decay trend associated to the LW is clear for the elements 1–5. This

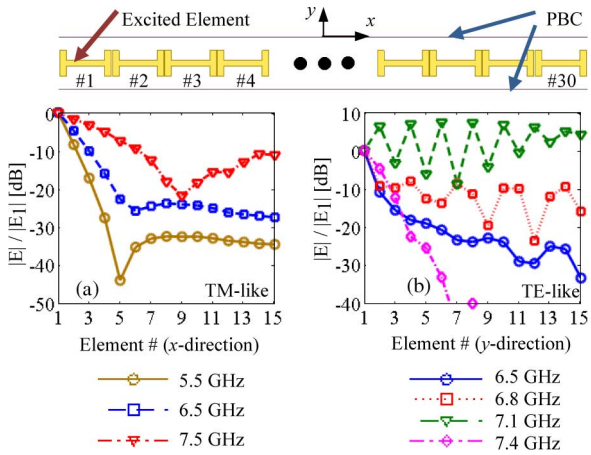

Fig. 8. Chain of 30 dogbones in the y-direction, surrounded by periodic boundary conditions (PBCs). Only element #1 is excited. (a) Field magnitude versus elements 1–15 along the x-direction. A clear exponential decay of the TM-like field is observed in the first five elements in all cases. (b) Analogous plot for field sampled at elements 1–15 along the y-direction, using PBCs in the x-direction, showing a guided mode at 7.1 GHz.

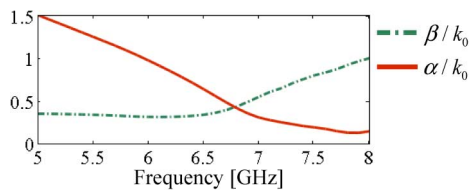

Fig. 9. Attenuation α and phase constant β of the TM-like LW ($\beta - j\alpha$) along the x-direction, which is dominant in the elements 1–5. They are normalized with respect to the free-space wavenumber $k_0 = \omega\sqrt{\varepsilon_0\mu_0}$.

analysis reveals that an LW is dominant at least in the first five dogbones for several considered frequencies.

The normalized phase and attenuation constants ($\beta - j\alpha$) of the dominant LW along x are plotted in Fig. 9 by curve-fitting the electric field sampled at each of the first five dogbones, #1–#5. The phase constant β of this LW is smaller than that of free space until 8 GHz, thus clearly this mode is in the fast-wave region (i.e., it is an LW.) The attenuation constant α decreases as the frequency increases, whereas the phase constant β has the opposite relation. This causes beam splitting in E-plane, which decreases the broadside gain as the frequency increases. At lower frequencies, the currents on all the dogbones are almost in phase, and the current magnitudes decay rapidly, which results in lower broadside gain, as clearly explained in [12]. Note that at 6.6 GHz, $\beta \approx \alpha < k_0$, which has been indicated as the optimum condition for an LW broadside beam [12]. The plot in Fig. 8 also shows the field along the y-direction for a periodic HIS with 30 elements along y, and PBCs along x, with only the first element fed. A bound mode is traveling for a narrow frequency band around 7.1 GHz (in agreement with [10]), causing the out-of-phase excitation of parallel chains, and thus the drop of broadside gain around 7 GHz for Case A.

III. Conclusion

HISs can be used as direct radiators without any dipole on top. The presence of a usable leaky wave shows that HISs do not necessarily act simply as magnetic mirrors. The feeding in Case B has higher gain, reaching values of 9–12.6 dBi, and a better radiation pattern than Case A in the frequency band 6.7–7.6 GHz because of better excitation of the lateral dogbone chains. It is worth mentioning that Case-B designs can be also matched at frequencies of gain peak. Both designs A and B can be used in the band around 6 GHz, with gains on the order of 7.5 dB, comparable to what was achieved in [4], though in this letter we did not use a dipole on top of the HIS. It is for the sake of comparison that we have used the same HIS as in [4] with exact dogbone dimensions and more or less the same overall HIS size. However, other HIS designs (including tapering of dimensions) may offer even better performances, in terms of gain and bandwidth, to be explored. The excitation by a dipole may introduce degrees of freedom for input matching purposes. However, some extra capacitance to balance the inductive reactance shown in Figs. 5 and 7 can be easily inserted by modifying the metal layer near the excitation.

Acknowledgment

The authors are grateful to Ansys for providing the simulation tools (HFSS and Ansoft Designer) that were instrumental in the design process.

References

[1] Y. Fan and Y. Rahmat-Samii, "Reflection phase characterizations of the EBG ground plane for low profile wire antenna applications," *IEEE Trans. Antennas Propag.*, vol. 51, no. 10, pp. 2691–2703, Oct. 2003.

[2] H. Mosallaei and K. Sarabandi, "Antenna miniaturization and bandwidth enhancement using a reactive impedance substrate," *IEEE Trans. Antennas Propag.*, vol. 52, no. 9, pp. 2403–2414, Sep. 2004.

[3] S. Best and D. Hanna, "Design of a broadband dipole in close proximity to an EBG ground plane," *IEEE Antennas Propag. Mag.*, vol. 50, no. 6, pp. 52–64, Dec. 2008.

[4] A. Vallecchi, J. R. De Luis, F. Capolino, and F. De Flaviis, "Low profile fully planar folded dipole antenna on a high impedance surface," *IEEE Trans. Antennas Propag.*, vol. 60, no. 1, pp. 51–62, Jan. 2012.

[5] D. Sievenpiper, Z. Lijun, R. F. J. Broas, N. G. Alexopolous, and E. Yablonovitch, "High-impedance electromagnetic surfaces with a forbidden frequency band," *IEEE Trans. Microw. Theory Tech.*, vol. 47, no. 11, pp. 2059–2074, Nov. 1999.

[6] A. O. Karilainen, J. Vehmas, O. Luukkonen, and S. A. Tretyakov, "High-impedance-surface-based antenna with two orthogonal radiating modes," *IEEE Antennas Wireless Propag. Lett.*, vol. 10, pp. 247–250, 2011.

[7] O. Luukkonen, A. O. Karilainen, J. Vehmas, C. Simovski, and S. A. Tretyakov, "A high-impedance surface based antenna—Lose the antenna," in *Proc. 4th EuCAP*, 2010, pp. 1–5.

[8] C. Guclu, J. Sloan, S. Pan, and F. Capolino, "High impedance surface as an antenna without a dipole on top," in *Proc. IEEE APSURSI*, 2011, pp. 1028–1031.

[9] A. Vallecchi and F. Capolino, "Metamaterials based on pairs of tightly coupled scatterers," in *Theory and Phenomena of Metamaterials*, F. Capolino, Ed. Boca Raton, FL: CRC Press, 2009, p. 19.1.

[10] G. Donzelli, A. Vallecchi, F. Capolino, and A. Schuchinsky, "Metamaterial made of paired planar conductors: Particle resonances, phenomena and properties," *Metamaterials*, vol. 3, pp. 10–27, 2009.

[11] P. Baccarelli, F. Capolino, S. Paulotto, and A. B. Yakovlev, "In-plane modal analysis of a metalayer formed by arrayed pairs of dogbone-shaped conductors," *Metamaterials*, vol. 5, pp. 26–35, 2011.

[12] G. Lovat, P. Burghignoli, and D. R. Jackson, "Fundamental properties and optimization of broadside radiation from uniform leaky-wave antennas," *IEEE Trans. Antennas Propag.*, vol. 54, no. 5, pp. 1442–1452, May 2006.

[13] Z. Tianxia, D. R. Jackson, J. T. Williams, and A. A. Oliner, "General formulas for 2-D leaky-wave antennas," *IEEE Trans. Antennas Propag.*, vol. 53, no. 11, pp. 3525–3533, Nov. 2005.